



Oxidative degradation of nitrobenzene by a Fenton-like reaction with Fe-Cu bimetallic catalysts

Yang Sun^a, Zixu Yang^a, Pengfei Tian^a, Yiyi Sheng^a, Jing Xu^{a,*}, Yi-Fan Han^{a,b,*}

^a State Key Laboratory of Chemical Engineering, East China University of Science and Technology, Shanghai 200237, China

^b Research Center of Heterogeneous Catalysis and Engineering Sciences, School of Chemical Engineering and Energy, Zhengzhou University, Zhengzhou 450001, China



ARTICLE INFO

Keywords:

Fenton
Nitrobenzene degradation
Fe-Cu bimetallic catalysts
Hydroxyl radicals
Mechanism

ABSTRACT

De-nitrogen of organic contaminants in industrial wastewater is a great challenge for environmental remediation. In this work, alumina-supported bimetallic Fe-Cu catalysts were synthesized using a sol-gel method and exhibited high performance in catalytic degradation of nitrobenzene (NB). The bimetallic 5Fe2.5Cu-Al₂O₃ catalyst showed a 100% NB (100 ppm) removal within 1 h, which was superior to the NB degradation efficiency over monometallic Fe and Cu catalysts. With combination of the catalytic performance and the characterization results of X-ray photoelectron spectroscopy and H₂-temperature-programmed reduction, we proposed that the synergistic effect between Fe and Cu species played a vital role in promoting the reduction of Fe³⁺ to Fe²⁺, thus enhancing the generation of hydroxyl radicals (·OH) and the degradation efficiency of NB. To elucidate the degradation pathway, gas chromatography-mass spectrometry and dynamic ultraviolet-visible spectroscopy were used to detect the intermediates during the degradation process. The results indicated that the degradation predominantly occurred via electrophilic addition of aromatic ring by ·OH, followed by the ring opening reaction and mineralization reaction. Moreover, NB can be efficiently decomposed into less stable aniline, which is apt to degrade. This work has not only made significant progress on the development of high-performance catalysts for the degradation of NB, but also provided a deep understanding of the mechanism for NB degradation.

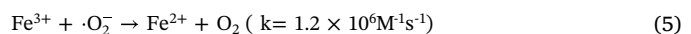
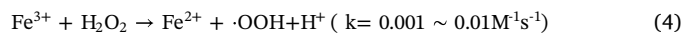
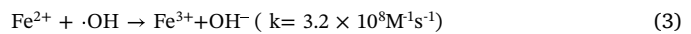
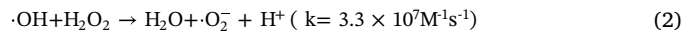
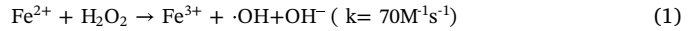
1. Introduction

Nitrobenzene (NB) is one of the major organic pollutants in water due to its wide use in explosives, dyes and insecticides, being notorious for its high toxicity, carcinogenicity and other adverse effects to organisms and environments. Moreover, NB shows poor activity toward oxidative degradation due to its strong electron-withdrawing characteristics of the nitro-group. The U.S. Environmental Protection Agency (EPA) regulates that NB levels in lakes and water streams should be no more than 17 ppm [1]. Thus, the awareness of environmental risks has spurred the development of efficient technologies for NB removal. The removal of NB by reducing it to less toxic aniline has been studied, but the living of aquatic creatures is still at risk once the level of aniline reaches to the environmental limit [2]. Therefore, the development of effective and environmental-friendly methods for NB degradation remains a great challenge.

Advanced oxidation processes (AOPs), such as the Fenton reaction, have been paid close attention for NB removal thanks to the non-selective and strong oxidative characteristics of hydroxyl radical (·OH)

[3,4]. In a traditional homogeneous Fenton system, ·OH is produced by the decomposition of hydrogen peroxide (H₂O₂) catalyzed by Fe²⁺. However, the homogeneous Fenton system suffers from massive production of undesired iron sludge which requires further separation step and may cause secondary contamination if not handled properly [5,6]. As an alternative, heterogeneous catalysts such as zero-valent iron (ZVI) [7] and iron oxide based catalysts [8–11] can overcome this issue, and they have been widely employed in the degradation of NB.

It is widely accepted that iron-based Fenton reaction consists of the following steps (Eqs. (1–5)):



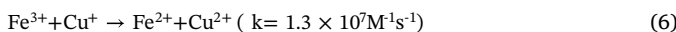
The reduction of Fe³⁺ to Fe²⁺ (Eq. (4)) with the lowest reaction rate

* Corresponding authors at: State Key Laboratory of Chemical Engineering, East China University of Science and Technology, Shanghai 200237, China.

E-mail addresses: xujing@ecust.edu.cn (J. Xu), yifanhan@ecust.edu.cn (Y.-F. Han).

constant (k) is the rate determining step of the whole catalytic cycle for ·OH generation [12]. Thus, acceleration of the reduction of Fe^{3+} is of vital importance for enhancing the degradation efficiency.

Bimetallic catalysts in some cases have better catalytic performance than their monometallic counterparts [6,9,13,14]. The superior catalytic performance of bimetallic catalysts was thought to be resulted from the increase in surface area and/or the synergistic effect between metals [15–17]. Recently, the role of interaction between iron and copper in a heterogeneous catalytic Fenton-like process has attracted much attention [18–20]. The Han's group [21] has measured the difference between oxidative and reductive potentials (ΔE) of redox cycles ($\text{Fe}^{3+}/\text{Fe}^{2+}$ and $\text{Cu}^{2+}/\text{Cu}^+$) in a monometallic Fe-AO-PAN and a bimetallic Cu-Fe-AO-PAN catalyst systems and found that the synergistic effect can be explained by the reduced ΔE for the $\text{Fe}^{3+}/\text{Fe}^{2+}$ redox cycle in Cu-Fe-AO-PAN. Zhang et al [22] has evidenced the existence of transformation from Fe^{3+} to Fe^{2+} during the catalytic process by detecting the chemical state of iron and copper species on the fresh and spent catalysts using X-ray photoelectron spectroscopy (XPS). The interaction between Fe and Cu (Eq. (6)) could lead to the rapid reduction of Fe^{3+}



Several previous studies on the bimetallic Fenton-like heterogeneous catalytic process were mainly focused on the degradation of phenols and dyes, which were more readily degraded than NB. In order to promote the catalytic cycle for ·OH generation, we developed a bimetallic Fe-Cu catalyst which exhibited extraordinary catalytic activity in NB degradation. The effects of operation conditions such as initial concentrations of H_2O_2 and NB in the feed, catalyst loading and reaction temperature on NB degradation performance were evaluated in detail. Finally, the degradation pathway of NB was proposed based on the identification of key intermediates by gas chromatography–mass spectrometry (GC-MS) and dynamic ultraviolet-visible (UV-vis) spectroscopy. We do believe the work presented here will inspire more ideals on the rational design of the Fenton-like solid catalysts for the oxidative degradation of N-containing organic pollutants.

2. Experimental

2.1. Reagents

Poly(ethylene glycol)-block-poly(propylene glycol)-block-poly(ethylene glycol) glycol Pluronic P123 was purchased from Sigma-Aldrich. Nitrate acid and anhydrous ethanol were provided by Shanghai Titan Technology Co., Ltd. Iron nitrate nonahydrate ($\text{Fe}(\text{NO}_3)_3 \cdot 9\text{H}_2\text{O}$), copper nitrate trihydrate ($\text{Cu}(\text{NO}_3)_2 \cdot 3\text{H}_2\text{O}$), aluminium nitrate nonahydrate ($\text{Al}(\text{NO}_3)_3 \cdot 9\text{H}_2\text{O}$), rhodamine B (RhB), methyl blue (MB), methyl orange (MO), phenol, bisphenol A (BPA), 4-chlorophenol (4CP), benzoic acid and toluene were purchased from Sinopharm Chemical Reagent Co., Ltd. Citric acid monohydrate, NB and H_2O_2 (30 wt %) were supplied by Shanghai Linfeng Chemical Reagent Co., Ltd. All chemicals and reagents were used as received without further treatment.

2.2. Catalyst preparation

A series of Fe-Cu bimetallic catalysts were prepared through a procedure reported by Fu et al. with a minor modification [23]. In a typical procedure, 2.0 g Pluronic P123 was dissolved in 20.0 mL ethanol and stirred for about 3 h. Meanwhile, 0.84 g of citric acid monohydrate, 0.40 g $\text{Fe}(\text{NO}_3)_3 \cdot 9\text{H}_2\text{O}$, 0.12 g $\text{Cu}(\text{NO}_3)_2 \cdot 3\text{H}_2\text{O}$, and 7.5 g Al ($\text{NO}_3)_3 \cdot 9\text{H}_2\text{O}$ (i.e. the loading ratio of Cu and Fe were 5 and 2.5 wt%) were dissolved in 20.0 mL of ethanol with vigorous stirring. Subsequently, the dissolved metal precursors were transferred into Pluronic P123 solution to form a mixed solution. The residual metal precursors were rinsed with additional 10.0 mL ethanol and transferred into the

abovementioned mixed solution. After being stirred for 5 h, the sol was dried and transformed into gel in oven under 333 K for 3 days. The resulting gel was calcined at 1023 K for 4 h to obtain the catalyst. Other Fe-Cu bimetallic catalysts with different metal loadings were also prepared. During preparation, the active metals may either incorporate into the framework of Al_2O_3 or dispersed as metal oxide particles on the surface of Al_2O_3 . For convenience, the as-prepared bimetallic catalysts were denoted as $x\text{Fe}y\text{Cu}-\text{Al}_2\text{O}_3$, where x and y represent the mass fraction of Fe and Cu, respectively. For comparison, monometallic catalysts were prepared using the same procedure.

2.3. Catalytic performance test

The degradation of NB and other model compounds was carried out in a series of thermostatic 200 mL batch reactors with a stirring rate of 720 rpm (the mass transfer effect was excluded) at specified temperatures. Each reactor was filled with a reaction solution that contained 88 mL deionized water and 10 mL NB (1000 ppm). 2 mL 0.1 M HNO_3 was added to the solution to adjust the initial pH value to 3. The catalyst was then added into the solution, and the suspension was vigorously stirred for 30 min to reach the adsorption-desorption equilibrium. After that, a certain amount of H_2O_2 (30 wt%) was added to initiate the reaction. At the given reaction time intervals, 3 mL supernatant solution was collected by filtration through a 0.22 μm Nafion membrane for the analysis of NB concentration and the leaching amount of metal ions. To evaluate the reusability of the catalyst, the spent catalyst from each experiment was collected, washed with deionized water, dried, and then reloaded in the reactor for recycling tests under the same conditions.

The concentration of NB in the reaction solution was determined by a HPLC (Altus A-10, PerkinElmer, Inc.) equipped with a PerkinElmer C18 Column (4.6 mm \times 150 mm, 5 μm) and a UV detector. The detection wavelength, column temperature, and flow rate were set at 280 nm, 40 °C, and 1.0 $\text{mL} \cdot \text{min}^{-1}$, respectively. The mobile phase included ultrapure water and methanol (vol/vol = 6/4). The concentration of other model contaminants (phenol, 4-Chlorophenol, bisphenol A and toluene) was determined by a HPLC or a UV-vis spectrometer. More details about the procedure of analysis were provided in supplementary material.

The GC-MS system was used to analyze the degraded products from the process [24]. The detailed description about sample preparation and analysis method were described in supplementary material.

The metal leaching was measured by ICP-MS (NexION 300X, PerkinElmer, Inc.). The concentration of ·OH was measured indirectly using benzoic acid as a probe molecule. The experiment procedure was adopted from literature [25].

2.4. Characterization

2.4.1. N_2 adsorption-desorption

The textural properties of the samples were evaluated by N_2 adsorption–desorption isotherms at 77 K using a physisorption analyzer (Micromeritics ASAP 2020). Prior to the analysis, the sample was degassed at 573 K for 6 h to remove any moisture and impurities. The surface area was calculated using the Brunauer–Emmett–Teller (BET) model for adsorption data obtained in a relative pressure range of 0.05–0.30. The pore size distribution was determined from the amount of N_2 adsorbed at a relative pressure of 0.99 by using the Barrett–Joyner–Halenda (BJH) algorithm. The average pore diameter of samples was determined by desorption branch according to the Barrett–Joyner–Halenda (BJH) model.

2.4.2. X-ray diffraction (XRD)

The XRD analysis of catalysts was performed on a Bruker D8-Advance X-ray powder diffractometer with a $\text{Cu K}\alpha$ ray source ($\lambda = 0.154 \text{ nm}$) at 40 kV and 40 mA. The XRD patterns were collected

over a 2θ range of 10–80° with a resolution of 0.02°.

2.4.3. Diffuse reflectance UV-vis (UV-vis DRS)

Diffuse reflectance UV-vis spectrum in the range of 200–800 nm were recorded on an UV-vis spectrophotometer (Lambda 750, PerkinElmer, Inc.) with BaSO₄ as a reference and were transformed into the Kubelka-Munk function, F(R).

2.4.4. Mössbauer spectrum

Mössbauer spectra were collected in a Wissel constant acceleration transmission mode with ⁵⁷Co/Rh source at 298 K. The data were curve-fitted using Lorentzian line shape function with a least-squares fitting procedure.

2.4.5. H₂ temperature-programmed-reduction (H₂-TPR)

H₂-TPR experiments were performed using a micro fixed-bed reactor (a quartz reactor with 20 cm in length and 0.4 cm in diameter). A thermal conductivity detector (TCD) was utilized to monitor the H₂ uptake. For each run, 50 mg of catalyst was loaded and purged with Ar (50 mL·min⁻¹) at 523 K for 1 h to remove the physisorbed moisture. After cooling to room temperature, the gas was switched to a 10 vol. % H₂/Ar flow (20 mL·min⁻¹) and the catalyst was purged until a stable baseline was obtained. Then, the catalyst could be reduced in the range of 473 K~1073 K with a ramping rate of 10 K·min⁻¹.

2.4.6. X-ray photoelectron spectroscopy (XPS)

XPS analysis was carried out on a Thermo Fisher Scientific ESCALAB 250Xi spectrometer with Al-Kα radiation ($\hbar\nu = 1486.6$ eV, pass energy : 40.0 eV) as the X-ray source. To compensate for surface charge effects, all the binding energies were calibrated using the C1s line at 284.60 eV.

3. Results and discussion

3.1. Catalytic performance test

3.1.1. Catalytic performance of xFeyCu-Al₂O₃

The NB removal efficiencies over various xFeyCu-Al₂O₃ catalysts were evaluated in an acidic solution (pH = 3.0). As shown in Fig. 1, 5Fe2.5Cu-Al₂O₃ exhibited the highest catalytic performance with a NB removal efficiency of 94% in 30 min, an indicative of a high catalytic activity in H₂O₂ activation. Compared with other catalyst systems, Fe-

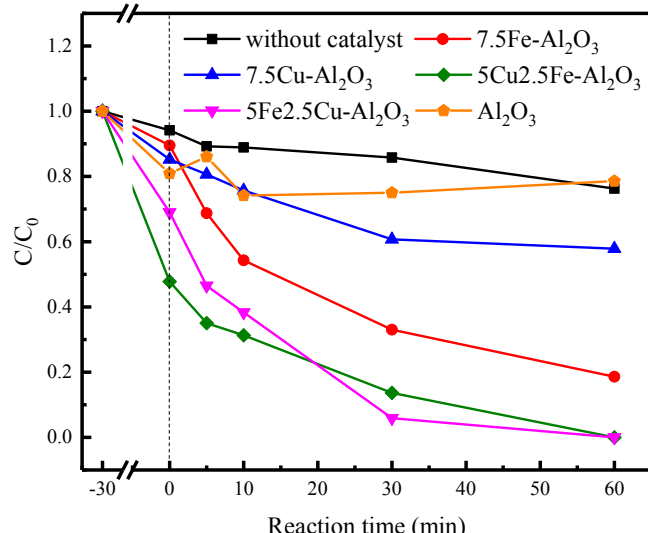


Fig. 1. Degradation performance of various catalysts (Reaction conditions: 323 K, 300 μL H₂O₂ (30%), 1 g·L⁻¹ catalyst, 100 ppm NB).

Table 1

Comparison of the performance of the xFeyCu-Al₂O₃ catalysts with state-of-the-art catalysts.

Catalyst	[NB] ₀ ^a (ppm)	NB Conversion (%)	Reaction Time (min)	Ref.
pyrite catalyst	20	80	300	[26]
Cu-AC	100	84	240	[27]
schwertmannite	50	92.5	30	[3]
kaolinite-supported zero-valent iron	39.8	82	250	[28]
5Fe2.5Cu-Al ₂ O ₃	100	94.1	30	This Work

^a The initial concentration of NB.

Cu bimetallic catalysts exhibited the highest the NB removal efficiency (Table 1) [3,26–28]. In addition, the bimetallic catalyst in this study possesses superior performance for NB removal compared with the monometallic catalysts (Table S1). It is noted that a mild NB removal was also observed over Al₂O₃ support only, and over monometallic catalysts. A slow removal rate (24% NB conversion in 1 h) was detected under noncatalytic conditions. Two monometallic catalysts, 7.5Fe-Al₂O₃ and 7.5Cu-Al₂O₃ showed NB removal of 65% and 40% in 60 min, respectively.

The difference in NB removal efficiencies between monometallic and bimetallic catalysts suggested a synergistic effect between Fe and Cu on NB removal. 5Cu2.5Fe-Al₂O₃ showed a lower reaction rate than 7.5Fe-Al₂O₃, implying that copper atoms may inhibit H₂O₂ decomposition in an acidic solution.

3.1.2. Effects of H₂O₂ dosage

The removal efficiency of NB over 5Fe2.5Cu-Al₂O₃ as a function of H₂O₂ dosage is shown in Fig. 2(a). The NB degradation efficiency measured at 10 min increased from 10.6% to 74.2% while H₂O₂ dosage increased from 100 μL to 400 μL. However, the further increase in H₂O₂ dosage led to a significant decrease in NB degradation efficiency. This phenomena can be explained by the dual function of H₂O₂ in the generation of 'OH radicals. On the one hand, higher H₂O₂ dosage favored the access of H₂O₂ molecules to the active sites, resulting in the generation of more 'OH radicals [29]. On the other hand, H₂O₂ could scavenge 'OH radicals to form less active 'O₂H radical (Eqs. (7)–(8)), leading to the loss of the activity in NB degradation



3.1.3. Effects of initial NB concentration

The influence of initial NB concentration on degradation efficiency is depicted in Fig. 2(b). As the initial NB concentration increased from 50 to 500 ppm, the NB removal efficiency in 10 min dropped sharply from 70.3% to 4.5%. It is generally accepted that the heterogeneous Fenton reaction occurs at the boundary zone between the catalyst surface and the solution, which involves the adsorption of targeted pollutants and H₂O₂ on the catalyst active sites, reaction of adsorbed molecules with 'OH generated by H₂O₂ decomposition, and desorption of products from the active sites of catalyst [1,14]. The competitive adsorption of NB and H₂O₂ on the catalyst surface significantly affected the degradation efficiency of NB. Variation of initial NB concentration at or below 100 ppm impacted little on the NB degradation efficiency because active sites were excess relative to the number of adsorbed NB molecules. The initial rise in NB concentration from 200 to 500 ppm is an indicative of the competitive adsorption of NB and H₂O₂. Consequently, the adsorption of H₂O₂ could be suppressed. Moreover, the accumulation of reaction intermediates on the catalyst surface may also block the adsorption of H₂O₂ [20,30].

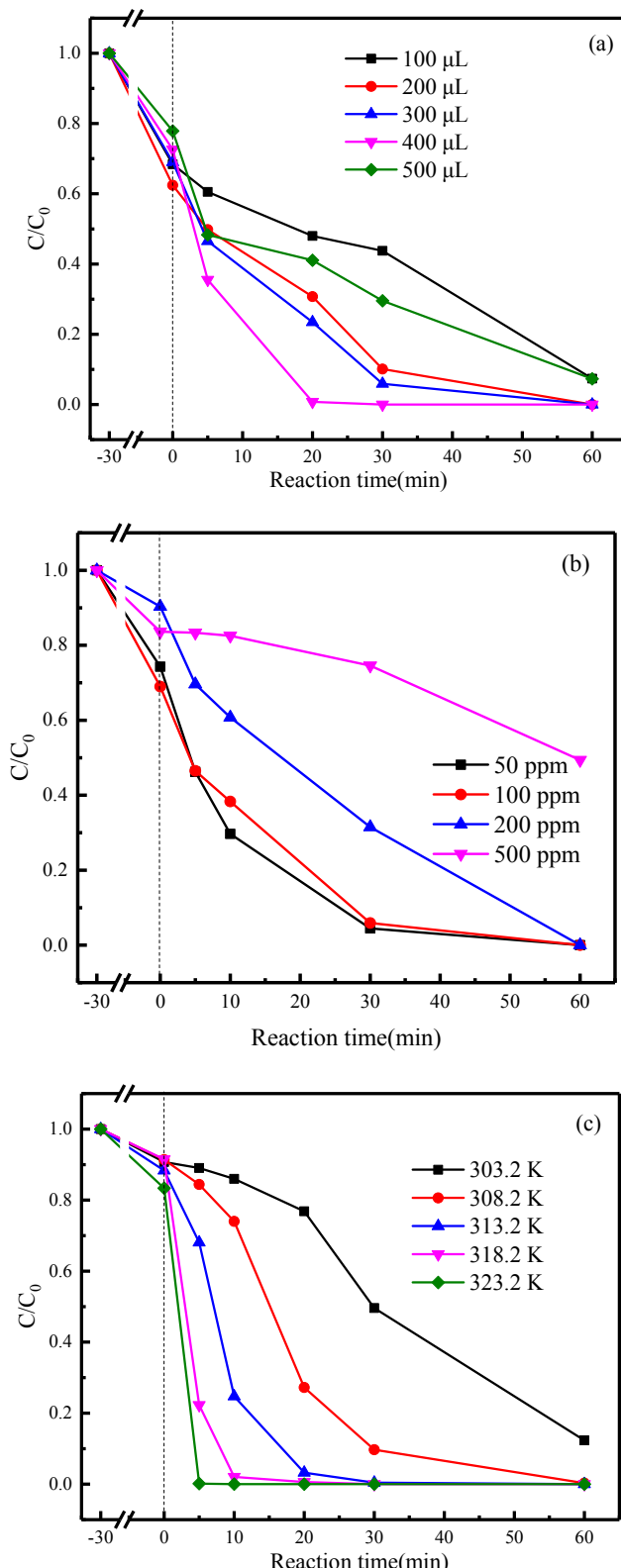


Fig. 2. The removal efficiency as a function of (a) H₂O₂ (30%) dosage (Reaction conditions: 323 K, 1 g·L⁻¹ 5Fe2.5Cu-Al₂O₃, 100 ppm NB), (b) initial NB concentration (Reaction conditions: 323 K, 300 µL H₂O₂ (30%), 1 g·L⁻¹ 5Fe2.5Cu-Al₂O₃), (c) reaction temperature (Reaction conditions: 300 µL H₂O₂ (30%), 0.5 g·L⁻¹ 5Fe2.5Cu-Al₂O₃, 100 ppm NB).

3.1.4. Effects of reaction temperature

Fenton reactions are typically temperature sensitive. As shown in Fig. 2(c), the NB removal efficiency showed an apparent positive trend toward the reaction temperature. For example, the NB removal obtained at 10 min corresponding to 303.2, 308.2, 313.2, 318.2, and 323.2 K was 14.0%, 26.0%, 75.3%, 97.9%, and 100%, respectively. Reaction temperature played an important role in controlling the kinetics. Raising temperature can obviously increase the rate constant, leading to the higher ·OH generation rate and NB degradation rate.

3.1.5. Effects of catalyst dosage

The removal efficiency has proved to be slightly increased when the catalyst dosage rose from 0.25 g·L⁻¹ to 0.5 g·L⁻¹, implying that the active sites were excess when the catalyst dosage was 0.25 g·L⁻¹ (Fig. S2). However, the NB removal efficiency showed a significant decline as the catalyst dosage further increased from 0.5 g·L⁻¹ to 2 g·L⁻¹. To investigate the effects of catalyst dosage on the NB removal efficiency, the generation rate of ·OH as a function of catalyst dosage was evaluated. Interestingly, the generation rate of ·OH increased as the catalyst dosage increased from 0.25 g·L⁻¹ to 0.5 g·L⁻¹, in agreement with the variation of the NB degradation rate. The generation rate of ·OH remained unchanged as the catalyst dosage increased to 1.0 g·L⁻¹. However, a further increase in catalyst dosage (2.0 g·L⁻¹) resulted in a significant decrease in the generation rate of ·OH due to the scavenger effect of H₂O₂ [30]. Based on these data, the optimum catalyst dosage for 5Fe2.5Cu-Al₂O₃ was estimated to be 0.5 g·L⁻¹.

3.1.6. Adaptability and reusability of 5Fe2.5Cu-Al₂O₃

To investigate the adaptability of 5Fe2.5Cu-Al₂O₃ in dealing with various pollutants, degradation experiments of selected model pollutants such as chemical dyes, phenols, and chloride-containing compounds were performed. As shown in Table 2, all the recalcitrant model pollutants were degraded substantially in 20 min. Particularly, the conversions (20 min) of 4CP (100 ppm), phenol (100 ppm), toluene (100 ppm) and MB (10 ppm) were all higher than 95%. The high removal rates of these model pollutants indicated that 5Fe2.5Cu-Al₂O₃ was capable of degrading various organic pollutants efficiently (Table 3).

Catalyst stability was evaluated by consecutive runs using the spent 5Fe2.5Cu-Al₂O₃ catalyst. The NB removal rate was recorded after 60 min. The results showed that the catalyst can be recycled for 4 times without significant activity loss (Fig. 3).

3.1.7. Qualitative and quantitative determination of ·OH

It is widely accepted that highly reactive ·OH is a predominant oxidative species in the Fenton reaction system. To validate the role of ·OH, excess t-butanol was added into the catalytic system as a ·OH scavenger. As illustrated in Fig. S3, negligible NB removal (~10%) was observed with addition of t-butanol. Meanwhile, we also measured the generation of ·OH. The total amount of ·OH generated in 60 min was 181.11 µM without t-butanol, compared to 16.52 µM with addition of t-butanol. We infer that ·OH was the predominant oxidative species in NB degradation.

Table 2

Degradation of various contaminants^a.

Entry	Contaminants	Initial conc. (ppm)	Conv. (20 min) (%)	Conv. (60 min) (%)
1	Methyl blue (MB)	10	99.72	100
2	Rhodamine B (RhB)	10	93.43	100
3	Methyl orange (MO)	10	78.56	100
4	Phenol	100	99.72	100
5	Bisphenol A	100	82.27	87.53
6	4-chlorophenol	100	96.54	98.12
7	Toluene	100	100	100

^a The initial H₂O₂ concentration is 1000 ppm.

Table 3
Textural properties of synthesized samples.

Sample	S_{BET} ($\text{m}^2 \text{g}^{-1}$) ^a	Pore diameter (nm)	Pore volume ($\text{cm}^3 \text{g}^{-1}$)
7.5Fe-Al ₂ O ₃	123	8.32	0.37
5Fe2.5Cu-Al ₂ O ₃	116	12.54	0.54
5Cu2.5Fe-Al ₂ O ₃	113	13.58	0.55
7.5Cu-Al ₂ O ₃	135	9.17	0.36
Al ₂ O ₃	137	6.40	0.33

^a The specific surface area.

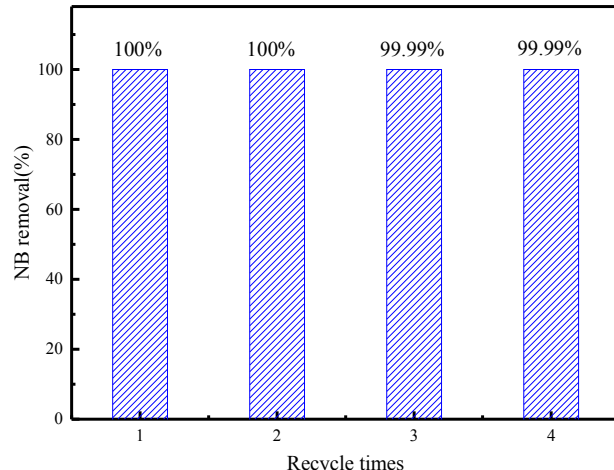


Fig. 3. Reusability of 5Fe2.5Cu-Al₂O₃ for NB degradation (Reaction conditions: 323 K, 300 μL H₂O₂ (30%), 0.5 g L^{-1} 5Fe2.5Cu-Al₂O₃).

3.2. Catalyst structure

To reveal the origin of the excellent performance of Fe-Cu bimetallic catalysts for NB degradation and ·OH generation, the catalysts were characterized using multiple characterization techniques. The specific surface areas of as-prepared catalysts and bare Al₂O₃ were determined through N₂-physisorption analysis. As shown in Fig. S4, all catalyst featured type IV isotherms with H1 hysteresis loop at the relative pressure P/P₀ = 0.42–0.98, corresponding to mesoporous material with cylindrical pores. Moreover, the catalyst possessed larger average pore volume than that of Al₂O₃ ($0.33 \text{ cm}^3 \text{g}^{-1}$), which suggested the formation of Fe-O-Al and Cu-O-Al structures that hindered the shrinkage of Al₂O₃ framework [31]. The BET surface area of Al₂O₃ is $137.10 \text{ m}^2 \text{g}^{-1}$, which decreased slightly to 122.98, 116.48, 112.77 and $135.28 \text{ m}^2 \text{g}^{-1}$ for 7.5Fe-Al₂O₃, 5Fe2.5Cu-Al₂O₃, 5Cu2.5Fe-Al₂O₃ and 7.5Cu-Al₂O₃, respectively. The decrease in the BET surface area after loading metals demonstrated the incorporation of Fe or Cu into Al₂O₃ framework [32–34], which was consistent with the previous studies [35].

The UV-Vis DRS spectra (Fig. 4) of xFe_xCu-Al₂O₃ catalysts displayed the morphologic properties and the states of Fe and Cu. No obvious signals were detected for pure Al₂O₃. Two major peaks for as-prepared catalysts appeared in UV region (218–248 nm) may be ascribed to the ligand to metal charge transfer (LMCT) between Fe/Cu species and oxygen lattice, revealing the presence of Fe-O-Al and Cu-O-Al in the Al₂O₃ frameworks, either tetrahedrally or octahedrally coordinated [36,37]. Moreover, the shoulder peaks at about 450 nm in the Vis region might result from the photo excited electron transition from O 2p level into the Fe 3d level of the iron oxide in the extra framework [38]. Meanwhile, a new broad peak in the range of 600–800 nm, assigned to the d-d transition of Cu²⁺, was observed with the addition of Cu. The increase in the peak intensity with the Cu loading amount indicates the presence of extra-framework copper oxide particles.

The peaks at 37.6°, 45.8° and 67.1° are ascribed to (311), (400) and (440) diffraction peaks of γ -Al₂O₃ (JCPDS No. 10–0425), respectively

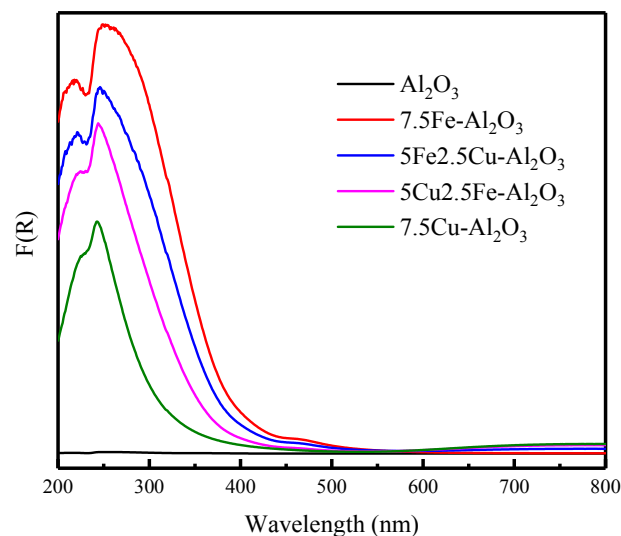


Fig. 4. UV-vis DRS spectra of the synthesized samples.

[39]. No diffraction peaks of iron oxide or copper oxide were observed in these samples, indicating that the formed Fe and Cu species were highly dispersed on Al₂O₃ [33]. After the doping of Fe or Cu, the calculated unit cell parameter (a_0) increased from the original 0.790 nm of Al₂O₃ to 0.792, 0.811, 0.798 and 0.792 nm of 7.5Fe-Al₂O₃, 7.5Cu-Al₂O₃, 5Fe2.5Cu-Al₂O₃ and 5Cu2.5Fe-Al₂O₃, respectively. Because the ionic radius of both Cu²⁺ and Fe³⁺ are larger than that of Al³⁺, the increase in a_0 may be caused by the replacement of Al³⁺ in γ -Al₂O₃ lattice accompanied with the formation of Cu-O-Al and Fe-O-Al.

⁵⁷Fe Mössbauer spectroscopy reveals the coordination environment of Fe species in catalysts. As shown in Fig. 5, for 7.5Fe-Al₂O₃, the presence of a broad paramagnetic doublet with a quadrupole splitting of 1.09 mm s^{-1} , a linewidth of 0.33 mm s^{-1} , and an isomer shift of 0.45 mm s^{-1} are characteristic features of the high-spin ferric iron in octahedral coordination (to O and OH ligands), demonstrating the presence of Fe-O-Al in the Al₂O₃ framework [40,41]. This is consistent with the results of BET, XRD and UV-vis. Notably, for bimetallic catalysts, the isomer shift which depends strongly on the electronic valence state decreased to 0.32, indicating the introduction of Cu atoms changed the electron density around Fe species [42,43].

The leaching of active components from 5Fe2.5Cu-Al₂O₃ was determined by measuring the concentration of ions of Fe and Cu in the solution using ICP-MS. The concentrations of Fe and Cu were 0.2 and 3.6 ppm, respectively, indicating negligible leaching of metal species. Yang et al. [44] reported that the leaching concentration of Fe and Cu after 120 min reaction were 0.6 and 32.8 ppm under the similar reaction conditions, respectively, which were much higher than our work. Such serious metal leaching led to the loss of activity of CuO-Fe₃O₄ catalyst in an acidic reaction environment ($\text{pH}_0 = 2.5$). The active metal atoms of 5Fe2.5Cu-Al₂O₃ in this work was firmly anchored into the Al₂O₃ matrix, and therefore they can barely escape from the catalyst due to the strong interaction of Cu-O-Al and Fe-O-Al, leading to an excellent stability even at acidic conditions. In addition, XPS analysis in Table 4 showed that surface Fe and Cu concentrations were much lower than their theoretical values, also suggesting that Fe and Cu species were highly dispersed into the bulk matrix, which was consistent with the results of BET, XRD, Mössbauer and UV-vis DRS.

3.3. The electronic interaction between Cu and Fe

A decrease in isomer shift of 5Fe2.5Cu-Al₂O₃ from Mössbauer spectra indicated the fact that the excellent catalytic performance of 5Fe2.5Cu-Al₂O₃ was due to the modification of electronic properties of iron species. In order to reveal the effect of Cu addition on the

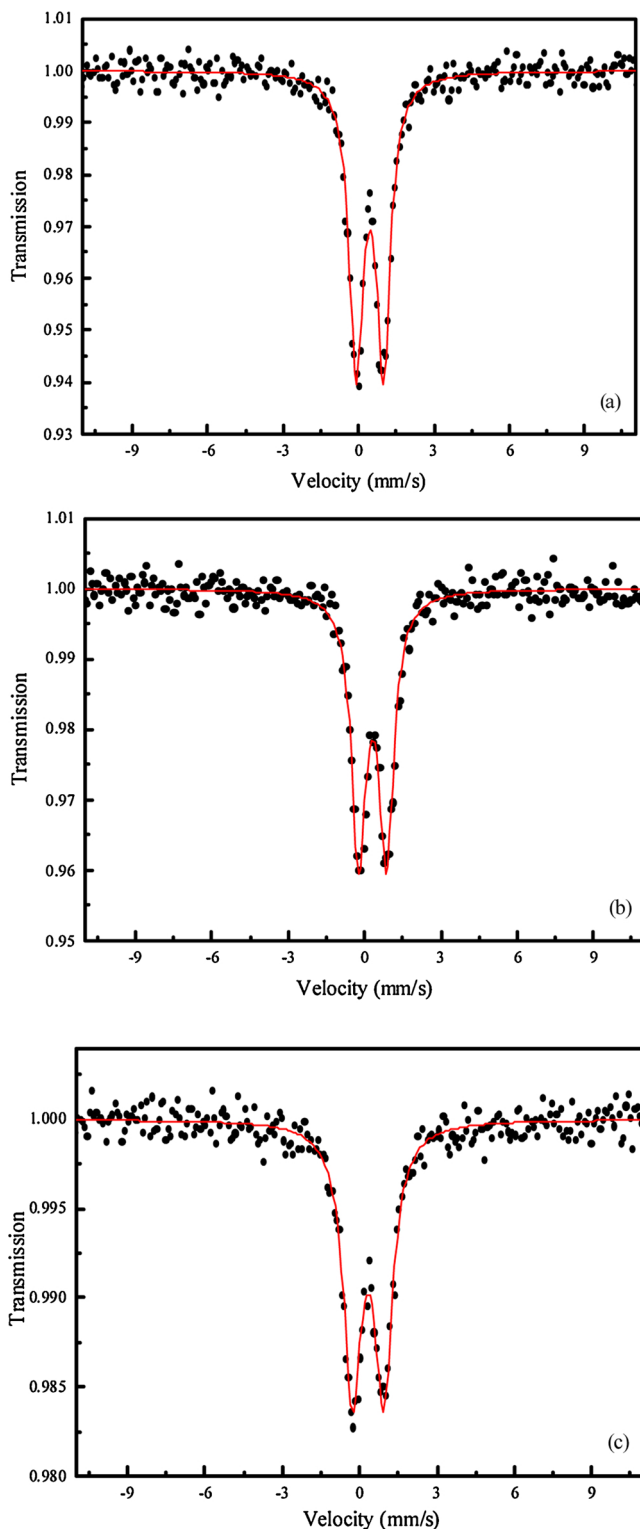


Fig. 5. Mössbauer spectrum of as-prepared Fe catalysts (a) 7.5Fe-Al₂O₃ (b) 5Fe2.5Cu-Al₂O₃ (c) 5Cu2.5Fe-Al₂O₃.

electronic properties of Fe species, the catalysts were characterized by H₂-TPR and XPS.

3.3.1. H₂-TPR

For 7.5Fe-Al₂O₃, the shoulder at 645 K is assigned to the reduction of iron oxide in the extra framework to Fe₃O₄, whereas the peak at 730 K is assigned to the reduction of Fe-O-Al to Fe₃O₄, so the reduction

Table 4

Ratio of atomic concentrations of elements calculated from XPS data on various catalysts.

Sample	Atomic concentration %				
	Al	Fe	Cu	O	C
7.5Fe-Al ₂ O ₃	29.64	2.61	0	58.39	9.36
5Fe2.5Cu-Al ₂ O ₃	31.43	1.35	1.60	55.64	9.98
5Cu2.5Fe-Al ₂ O ₃	31.91	0.89	2.37	55.81	9.02
7.5Cu-Al ₂ O ₃	31.37	0	1.25	58.41	8.97

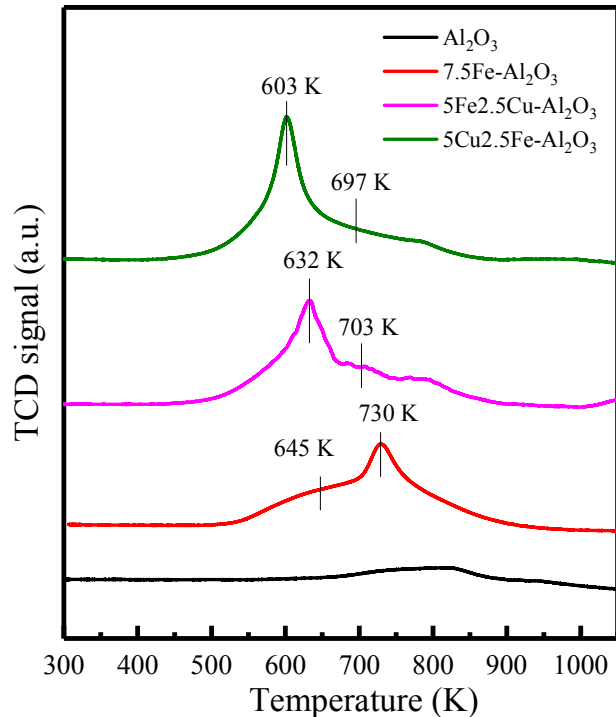


Fig. 6. H₂-TPR profiles of as prepared catalysts.

of Fe³⁺ ends at Fe²⁺ rather than Fe⁰ (Fig. 6). Previous studies have proposed that FeO phase could be stabilized on the support due to the strong Fe-Al₂O₃ interaction, which could further retard the transformation of FeO to Fe [45]. For 7.5Cu-Al₂O₃ (Fig. S6), the peaks at 521 K were due to a stepwise reduction of Cu²⁺ → Cu⁺ → Cu⁰ [23].

For bimetallic Fe-Cu catalysts, the reduction peaks were characterized by overlay peaks instead of the peaks corresponding to pure Fe or Cu species, which suggests the strong interaction between Fe species and Cu species. In addition, for 5Fe2.5Cu-Al₂O₃, the peak corresponding to the reduction of Cu²⁺ and the iron oxide in the extra framework to Cu⁰ and Fe₃O₄ (632 K) and the peak corresponding to the reduction of Fe-O-Al to Fe₃O₄ (703 K) shifted down to the lower temperatures compared to 7.5Fe-Al₂O₃ (645 K and 730 K). With further increasing the Cu/Fe ratio to 5/2.5, the reduction peaks of 5Cu2.5Fe-Al₂O₃ further dropped to 603 K and 697 K. This observation demonstrated that the reducibility of Cu²⁺ was decreased due to the strong interaction between Fe and Cu, which agreed well with previous work [46].

3.3.2. XPS

In XPS spectra, four peaks at 711.0, 712.9, 724.6 and 726.5 eV (Fig. 7(a)), assigned to Fe²⁺ 2p_{3/2}, Fe³⁺ 2p_{3/2}, Fe²⁺ 2p_{1/2} and Fe³⁺ 2p_{1/2}, respectively, were observed for 7.5Fe-Al₂O₃, indicating that this catalyst is composed of Fe²⁺ and Fe³⁺ species. For 7.5Cu-Al₂O₃ (Fig. 7(b)), the deconvolution of the primary peak revealed the

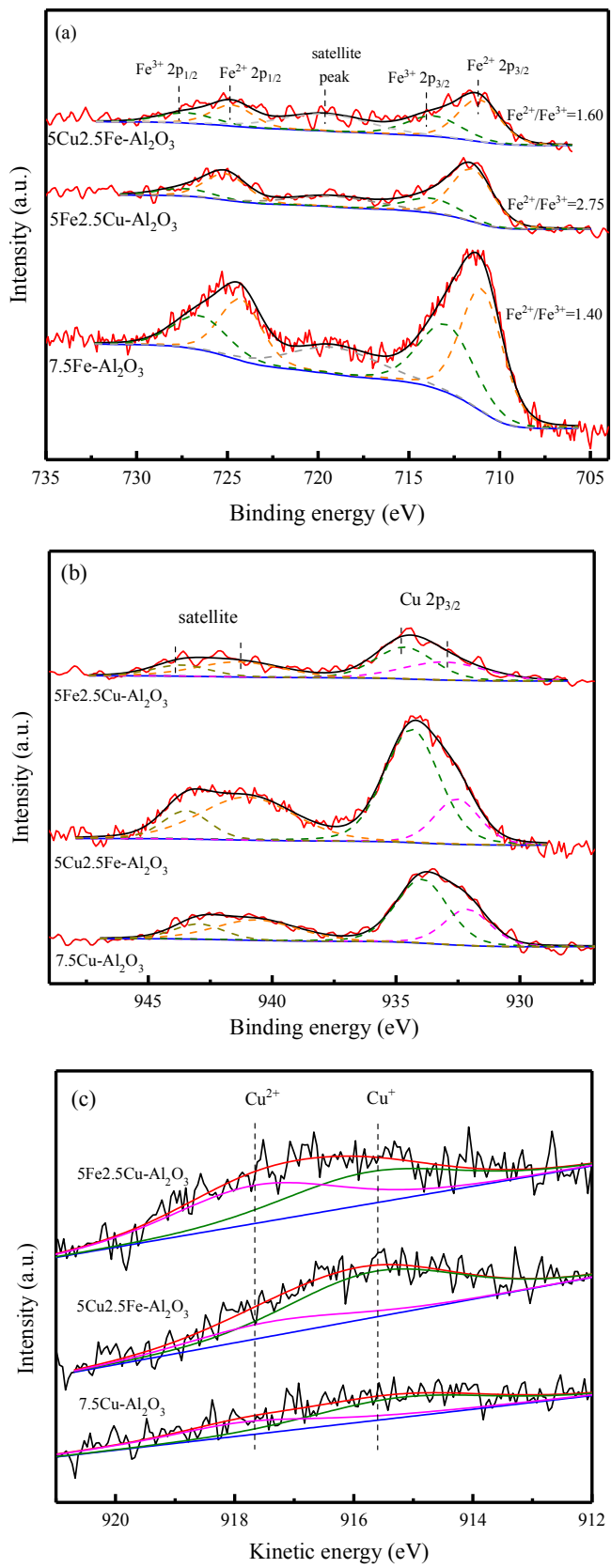


Fig. 7. XPS spectra of synthesized samples. (a) Fe 2p, (b) Cu 2p, (c) Cu LMM.

presence of two kinds of copper species. The higher Cu 2p_{3/2} BE of 934.8 eV and the shake-up peak at ca. 941.3–943.9 eV are two major XPS characteristics of Cu²⁺ species; in contrast, the reduced Cu species

Table 5
The I_{sat}/I_{pp} value of copper species of various catalysts.

Catalyst	I _{sat} /I _{pp}
7.5Cu-Al ₂ O ₃	0.75
5Cu2.5Fe-Al ₂ O ₃	0.48
5Fe2.5Cu-Al ₂ O ₃	0.95

(i.e. Cu⁺ and Cu⁰) show the lower Cu 2p_{3/2} BE of 933.1 eV and absence of the shake-up peak. The XPS Cu 2p_{3/2} peaks of Cu⁰ and Cu⁺ were partially overlapped because their BE values are very close. To further identify the peak assignment of the Cu species, Auger Cu LMM lines were analyzed. As shown in Fig. 7(c), the kinetic energy (KE) at 915.6 and 917.6 eV could be assigned to Cu⁺ and Cu²⁺, respectively. Therefore, the peak at 933.1 eV could result from Cu⁺.

The peak intensity ratio of Fe²⁺/Fe³⁺ was calculated to be 1.40 for 7.5Fe-Al₂O₃. For the Fe-Cu bimetallic catalysts, the Fe²⁺/Fe³⁺ ratios increased to 1.60 and 2.75 for 5Cu2.5Fe-Al₂O₃ and 5Fe2.5Cu-Al₂O₃, respectively. This again evidenced that the concentration of Fe²⁺ in the as-prepared catalysts was remarkably enhanced by alloying Fe and Cu, manifesting the strong interaction between Fe and Cu. Moreover, as listed in Table 5, the intensity ratio of Cu²⁺ satellite peaks to Cu⁺ principal peaks (I_{sat}/I_{pp}) [47] were higher than that of pure Cu, suggesting that the reduction degree of Cu species was decreased by the Fe-Cu interaction, which was also supported by H₂-TPR result.

3.4. The structure-performance relationship

Both H₂-TPR and XPS results suggested that the reduction of Fe³⁺ to Fe²⁺, which is the rate-determining step for ·OH production over monometallic Fe catalysts (Eq. 4), was significantly enhanced by alloying Fe and Cu. Accordingly, we assume that the Cu species in Fe-Cu bimetallic catalysts promoted the reduction of Fe³⁺ to Fe²⁺, then accelerated the catalytic cycle of the production of ·OH, which is predominant oxidative species in the Fenton reaction system, and eventually enhanced the degradation of NB. We believe that the excellent performance of 5Fe2.5Cu-Al₂O₃ was mainly due to its important role in catalyzing the reduction of Fe³⁺.

To verify our hypothesis, the quantitative determination of ·OH was carried out. Fig. 8 shows that the total amount of ·OH produced over 5Fe2.5Cu-Al₂O₃ (174.4 μM) was much higher than that over 7.5Fe-Al₂O₃ (138.9 μM), it has proved our assumption. Since the reduction of

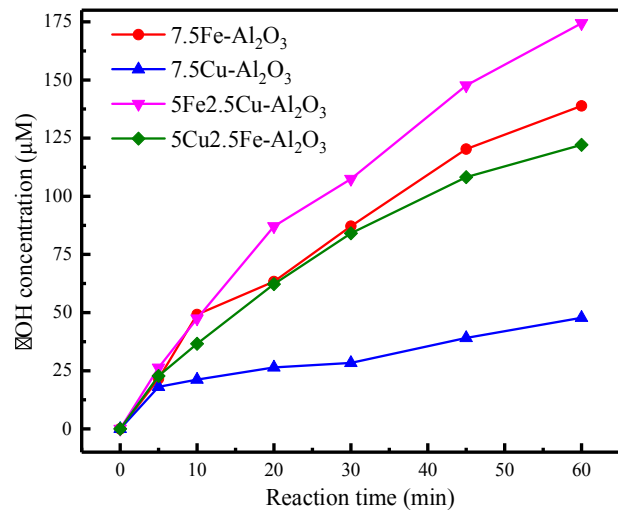
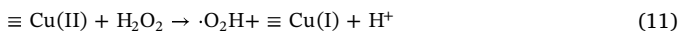
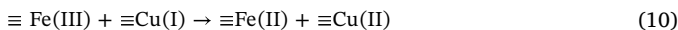
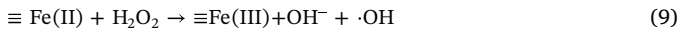


Fig. 8. The concentration of generated ·OH using different catalysts (Reaction conditions: 323 K, 300 μL H₂O₂ (30%), 1 g L⁻¹ catalyst, 1500 ppm benzoic acid).

Fe^{3+} by Cu^+ (Eqs. (6)) is more readily than Fe^{3+} by H_2O_2 (Eqs. (4)), we proposed that the Fe^{2+} species of Fe-Cu bimetallic catalyst is regenerated through the reaction between Fe^{3+} and Cu^+ instead of the reduction of Fe^{3+} by H_2O_2 , as listed in the Eqs (9)–(11):



As a result, the overall rate of generated $\cdot\text{OH}$ is markedly increased, 5Fe2.5Cu-Al₂O₃ can be applied for the high-efficiency treatment of NB in the Fenton process.

3.5. Reaction pathway of NB degradation

To reveal the mechanism of NB degradation over Fe-Cu catalysts, we studied the degradation pathway via probing the unstable intermediates using UV-vis spectrum and GC-MS.

3.5.1. Dynamic NB degradation process

The UV-vis spectra of NB during the degradation process over 5Fe2.5Cu-Al₂O₃ are illustrated in Fig. 9. The characteristic absorption band of NB at 294 nm diminished quickly, along with concomitant tiny hypsochromic shifting from 294 to 283 nm, this fact hints the p- π conjugation effect and π - π conjugation effect of NB were eliminated. Meanwhile, the absorbance in the region of 390~500 nm increased within the initial 20 min and then decreased to ~ 0 , and it suggests the generation and then disappearance of yellow intermediates.

3.5.2. Intermediates

The chemical oxidation treatment of wastewater comprises three key steps: (i) pre-oxidation to remove the inorganic compounds, color, taste, odor, turbidity, and suspended solids, (ii) intermediate oxidation for degrading micropollutants and trihalomethane precursors to improve the biodegradability of water, and (iii) final disinfection to provide drinking water. Since the Fenton-like reaction is usually followed by biological treatments, the biocompatibility and biodegradability of the intermediate is of vital importance in the whole remediation process. Generally, the degradation of NB via the Fenton-like system can occur through the following three pathways: (i) NB is attacked directly by $\cdot\text{OH}$ on the *ipso* position and form NO_2^- and benzene radicals; (ii) $\cdot\text{OH}$ reacts with aromatic ring by electrophilic addition to generate 2-nitrophenol, 3-nitrophenol, and 4-nitrophenol; (iii) reductive degradation of NB in presence of Fe^{2+} in an acid solution with aniline as the end-product, which is more biodegradable than NB.

Finally, all the intermediates are transformed into CO_2 , HNO_3 , and

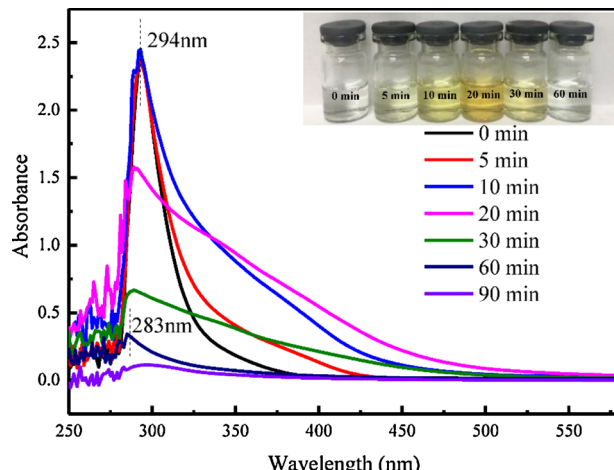


Fig. 9. UV-vis absorption spectra over 5Fe2.5Cu-Al₂O₃ during the reaction time.

Table 6
Intermediate of NB degradation over 5Fe2.5Cu-Al₂O₃.

Retention time·min ⁻¹	Compound	Molecular weight	Chemical structure
5.026	<i>N</i> -Ethylmethylamine	59.11	<chem>CCN</chem>
5.495	Acetaldehyde	44.05	<chem>CC=O</chem>
5.500	Ethylene oxide	44.05	<chem>CC1=CO1</chem>
9.198	NB	123.11	<chem>O=[N+]([O-])c1ccccc1</chem>
9.935	2-Nitrophenol	139.11	<chem>Oc1ccc([N+]([O-])=O)cc1</chem>
14.169	3-Nitrophenol	139.11	<chem>Oc1ccc([N+]([O-])=O)cc1</chem>
14.638	4-Nitrophenol	139.11	<chem>Oc1ccc([N+]([O-])=O)cc1</chem>
13.106	Propanolamine	75.11	<chem>CCNCCCO</chem>

H_2O through ring cleavage and mineralization. To clarify the reaction pathway, we carried out an on-line analysis of the intermediate during NB degradation in 30 min using a GC-MS system. The identification results of these compounds were summarized in Table 6. The intermediates with high peak intensities are 2-nitrophenol, 3-nitrophenol, and 4-nitrophenol. Secondary contaminants that have been reported in literature, such as 1,3-dinitrobenzene whose toxicity was about 30 times higher than that of NB [48,49] were not detected. The missing of 1,3-dinitrobenzene is due to two possible reasons: (i) the deeper mineralization that transforms 1,3-dinitrobenzene into smaller molecules; (ii) the Cu doping prohibited the generation of 1,3-dinitrobenzene [50]. Combining our results with previous works [2,48,49,51–54], a plausible reaction pathway for NB degradation for the Fe-Cu bimetallic Fenton-like system was illustrated by Fig. 10. The GC-MS profiles proved the generation of various nitrophenols indicated by the yellow color of the intermediates. Therefore, the electrophilic attack on the benzene ring of NB was the predominant step. Finally, the above-mentioned intermediates eventually were decomposed to CO_2 and HNO_3 [55].

4. Conclusions

A series of novel Fe-Cu bimetallic doped alumina catalysts were prepared via a facile sol-gel method and showed high performance in the Fenton-like reaction for NB degradation. ca.100% NB was removed within 1 h in the presence of 5Fe2.5Cu-Al₂O₃ and H_2O_2 . Furthermore, 5Fe2.5Cu-Al₂O₃ also exhibited high activity for removal of various organic pollutants. According to BET, XRD, Mössbauer and UV-vis DRS results, the doped metal ions were highly dispersed in both the framework and the extra-framework of mesoporous alumina. H₂-TPR and XPS indicated that Cu species promoted the reduction of Fe^{3+} to Fe^{2+} , which is the active site for the generation of $\cdot\text{OH}$ that is responsible for NB degradation. UV-vis spectra and GC-MS results confirmed that no stable highly toxic 1,3-dinitrobenzene existed throughout the reaction, indicating that this catalytic system can also be readily coupled with a biodegradation process in the practical application. Finally, a possible degradation mechanism that involves the opening of aromatic ring by

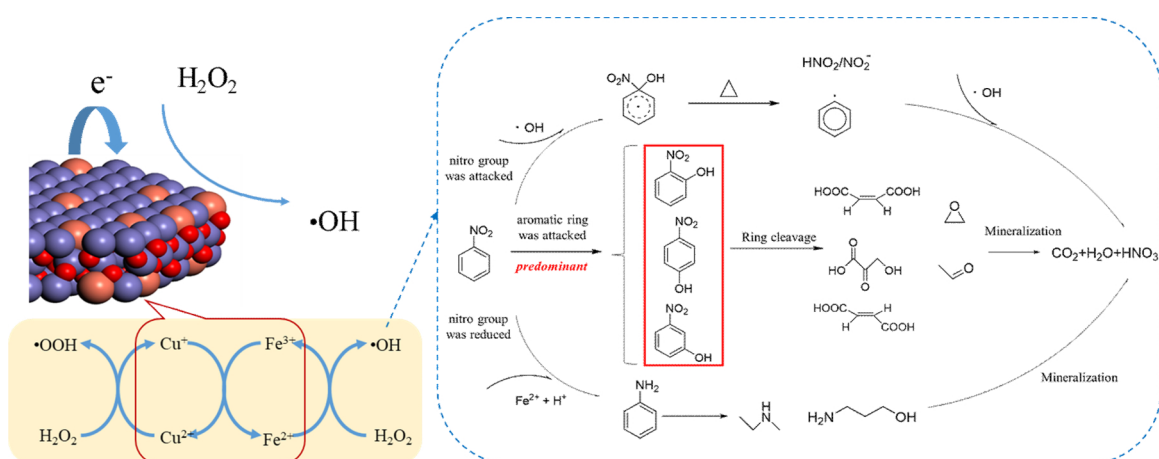


Fig. 10. Proposed possible mechanism of NB degradation over 5Fe2.5Cu-Al₂O₃ in the presence of H₂O₂.

electrophilic addition and reductive degradation of nitro group was proposed. Our findings not only provide new insights into the rational design of high-performance bimetallic Fenton-like catalysts for nitrogen containing pollutant degradation, but also give inspiration to the research involving catalytic oxidation reactions.

Acknowledgements

The authors are grateful to the support from the National Key R&D Program of China (2018YFB0605803), National Natural Science Foundation of China (21808057 and U1463205), Fundamental Research Funds for the Central Universities (222201718002), and Innovation Scientists and Technicians Troop Construction Projects of Henan Province.

Appendix A. Supplementary data

Supplementary material related to this article can be found, in the online version, at doi:<https://doi.org/10.1016/j.apcatb.2018.11.009>.

References

- [1] L. Sun, H. Song, Q. Li, A. Li, Fe/Cu bimetallic catalysis for reductive degradation of nitrobenzene under oxic conditions, *Chem. Eng. J.* 283 (2016) 366–374.
- [2] Y. Mu, H.Q. Yu, J.C. Zheng, S.J. Zhang, G.P. Sheng, Reductive degradation of nitrobenzene in aqueous solution by zero-valent iron, *Chemosphere* 54 (2004) 789–794.
- [3] H. Duan, Y. Liu, X. Yin, J. Bai, J. Qi, Degradation of nitrobenzene by Fenton-like reaction in a H₂O₂/schwertmannite system, *Chem. Eng. J.* 283 (2016) 873–879.
- [4] S. Xu, H. Zhu, W. Cao, Z. Wen, J. Wang, C.P. François-Xavier, T. Wintgens, Cu-Al₂O₃-g-C₃N₄ and Cu-Al₂O₃-C-dots with dual-reaction centres for simultaneous enhancement of Fenton-like catalytic activity and selective H₂O₂ conversion to hydroxyl radicals, *Appl. Catal. B-Environ.* 234 (2018) 223–233.
- [5] M. Dükkanç, G. Gündüz, S. Yılmaz, R.V. Prihod'ko, Heterogeneous Fenton-like degradation of Rhodamine 6G in water using CuFeZSM-5 zeolite catalyst prepared by hydrothermal synthesis, *J. Hazard. Mater.* 181 (2010) 343–350.
- [6] M. Xia, M. Long, Y. Yang, C. Chen, W. Cai, B. Zhou, A highly active bimetallic oxides catalyst supported on Al-containing MCM-41 for Fenton oxidation of phenol solution, *Appl. Catal. B-Environ.* 110 (2011) 118–125.
- [7] Y. Segura, F. Martínez, J.A. Melero, Effective pharmaceutical wastewater degradation by Fenton oxidation with zero-valent iron, *Appl. Catal. B-Environ.* 136–137 (2013) 64–69.
- [8] P. Massa, A. Dafinov, F.M. Cabello, R. Fenoglio, Catalytic wet peroxide oxidation of phenolic solutions over Fe₂O₃/CeO₂ and WO₃/CeO₂ catalyst systems, *Catal. Commun.* 9 (2008) 1533–1538.
- [9] Z. Xie, C. Wang, L. Yin, Nickel-assisted iron oxide catalysts for the enhanced degradation of refractory DDT in heterogeneous Fenton-like system, *J. Catal.* 353 (2017) 11–18.
- [10] J.V. Coelho, M.S. Guedes, R.G. Prado, J. Tronto, J.D. Ardisson, M.C. Pereira, L.C.A. Oliveira, Effect of iron precursor on the Fenton-like activity of Fe₂O₃/mesoporous silica catalysts prepared under mild conditions, *Appl. Catal. B-Environ.* 144 (2014) 792–799.
- [11] R.C.C. Costa, F.C.C. Moura, J.D. Ardisson, J.D. Fabris, R.M. Lago, Highly active heterogeneous Fenton-like systems based on Fe⁰/Fe₃O₄ composites prepared by controlled reduction of iron oxides, *Appl. Catal. B-Environ.* 83 (2008) 131–139.
- [12] T. Rigg, W. Taylor, J. Weiss, The rate constant of the reaction between hydrogen peroxide and ferrous ions, *J. Chem. Phys.* 22 (1954) 575–577.
- [13] X. Li, W. Liu, J. Ma, Y. Wen, Z. Wu, High catalytic activity of magnetic FeO_x/NiO_y/SBA-15: the role of Ni in the bimetallic oxides at the nanometer level, *Appl. Catal. B-Environ.* 179 (2015) 239–248.
- [14] S. Karthikeyan, M.P. Pachamuthu, M.A. Isaacs, S. Kumar, A.F. Lee, G. Sekaran, Cu and Fe oxides dispersed on SBA-15: a Fenton type bimetallic catalyst for N,N-diethyl-p-phenyl diamine degradation, *Appl. Catal. B-Environ.* 199 (2016) 323–330.
- [15] T. Xu, G. He, Y. Zhao, H. Gu, Z. Jiang, Q. Chen, X. Sun, H. Chen, Benzenoid-like CuFeO₂@reduced graphene oxide: facile synthesis and its excellent catalytic performance in selective oxidation, *Appl. Surf. Sci.* 389 (2016) 840–848.
- [16] M. Dükkanç, G. Gündüz, S. Yılmaz, Y.C. Yaman, R.V. Prihod'ko, I.V. Stolyarova, Characterization and catalytic activity of CuFeZSM-5 catalysts for oxidative degradation of Rhodamine 6G in aqueous solutions, *Appl. Catal. B-Environ.* 95 (2010) 270–278. A. Fortuny, C.
- [17] M. Danish, X. Gu, S. Lu, A. Ahmad, M. Naqvi, U. Farooq, X. Zhang, X. Fu, Z. Miao, Y. Xue, Efficient transformation of trichloroethylene activated through sodium percarbonate using heterogeneous zeolite supported nano zero valent iron-copper bimetallic composite, *Chem. Eng. J.* 308 (2017) 396–407.
- [18] W.R.P. Barros, J.R. Steer, M.R.V. Lanza, A.C. Tavares, Catalytic activity of Fe_{3-x}Cu_xO₄ (0 ≤ x ≤ 0.25) nanoparticles for the degradation of amaranth food dye by heterogeneous electro-Fenton process, *Appl. Catal. B-Environ.* 180 (2016) 434–441.
- [19] A.F. Rossi, R.C. Martins, R.M. Quinta-Ferreira, Composition effect of iron–copper composite catalysts in the Fenton heterogeneous process efficiency and cooxidation synergy assessment, *Ind. Eng. Chem. Res.* 53 (2014) 15369–15373.
- [20] Y. Feng, C. Liao, K. Shih, Copper-promoted circumneutral activation of H₂O₂ by magnetic CuFe₂O₄ spinel nanoparticles: mechanism, stoichiometric efficiency, and pathway of degrading sulfanilamide, *Chemosphere* 154 (2016) 573–582.
- [21] Z. Han, Y. Dong, S. Dong, Copper–iron bimetal modified PAN fiber complexes as novel heterogeneous Fenton catalysts for degradation of organic dye under visible light irradiation, *J. Hazard. Mater.* 189 (2011) 241–248.
- [22] X. Zhang, Y. Ding, H. Tang, X. Han, L. Zhu, N. Wang, Degradation of bisphenol A by hydrogen peroxide activated with CuFeO₂ microparticles as a heterogeneous Fenton-like catalyst: efficiency, stability and mechanism, *Chem. Eng. J.* 236 (2014) 251–262.
- [23] L. Fu, X. Li, M. Liu, H. Yang, Insights into the nature of Cu doping in amorphous mesoporous alumina, *J. Mater. Chem. A* 1 (2013) 14592–14605.
- [24] Y. Zhang, H. Lei, Z. Yang, K. Qian, E. Villota, Renewable high-purity mono-phenol production from catalytic microwave-induced pyrolysis of cellulose over biomass-derived activated carbon catalyst, *ACS Sustain. Chem. Eng.* (2018).
- [25] M.E. Lindsey, M.A. Tarr, Quantitation of hydroxyl radical during Fenton oxidation following a single addition of iron and peroxide, *Chemosphere* 41 (2000) 409–417.
- [26] Y. Zhang, K. Zhang, C. Dai, X. Zhou, H. Si, An enhanced Fenton reaction catalyzed by natural heterogeneous pyrite for nitrobenzene degradation in an aqueous solution, *Chem. Eng. J.* 244 (2014) 438–445.
- [27] Priyanka V. Subbaramaiah, V.C. Srivastava, I.D. Mall, Catalytic oxidation of nitrobenzene by copper loaded activated carbon, *Sep. Purif. Technol.* 125 (2014) 284–290.
- [28] Y. Wu, H. Yao, S. Khan, S. Hu, L. Wang, Characteristics and mechanisms of kaolinite-supported zero-valent iron/H₂O₂ system for nitrobenzene degradation, *Clean-Sol Air Water* 45 (2017) 1600826.
- [29] X. Yang, P.-F. Tian, C. Zhang, Y.-q. Deng, J. Xu, J. Gong, Y.-F. Han, Au/carbon as Fenton-like catalysts for the oxidative degradation of bisphenol A, *Appl. Catal. B-Environ.* 134 (2013) 145–152.
- [30] J. Wang, C. Liu, J. Li, R. Luo, X. Hu, X. Sun, J. Shen, W. Han, L. Wang, In-situ incorporation of iron–copper bimetallic particles in electrospun carbon nanofibers as an efficient Fenton catalyst, *Appl. Catal. B-Environ.* 207 (2017) 316–325.
- [31] Y. Wang, H. Zhao, G. Zhao, Iron–copper bimetallic nanoparticles embedded within ordered mesoporous carbon as effective and stable heterogeneous Fenton catalyst

for the degradation of organic contaminants, *Appl. Catal. B-Environ.* 164 (2015) 396–406.

[32] L. Lyu, L. Zhang, Q. Wang, Y. Nie, C. Hu, Enhanced Fenton catalytic efficiency of γ -Cu-Al₂O₃ by σ -Cu²⁺-Ligand complexes from aromatic pollutant degradation, *Environ. Sci. Technol.* 49 (2015) 8639–8647.

[33] L. Lyu, L. Zhang, C. Hu, Enhanced Fenton-like degradation of pharmaceuticals over framework copper species in copper-doped mesoporous silica microspheres, *Chem. Eng. J.* 274 (2015) 298–306.

[34] M.P. Pachamuthu, S. Karthikeyan, R. Maheswari, A.F. Lee, A. Ramanathan, Fenton-like degradation of Bisphenol A catalyzed by mesoporous Cu/TUD-1, *Appl. Surf. Sci.* 393 (2017) 67–73.

[35] B.K. Ghosh, S. Hazra, B. Naik, N.N. Ghosh, Preparation of Cu nanoparticle loaded SBA-15 and their excellent catalytic activity in reduction of variety of dyes, *Powder Technol.* 269 (2015) 371–378.

[36] G. Zhang, J. Long, X. Wang, Z. Zhang, W. Dai, P. Liu, Z. Li, L. Wu, X. Fu, Catalytic role of Cu sites of Cu/MCM-41 in phenol hydroxylation, *Langmuir* 26 (2010) 1362–1371.

[37] Z. Jia, W.C. Zhang, W.M. Wang, D. Habibi, L.C. Zhang, Amorphous Fe₇₈Si₉B₃alloy: An efficient and reusable photo-enhanced Fenton-like catalyst in degradation of cibacron brilliant red 3B-A dye under UV-vis light, *Appl. Catal. B-Environ.* 192 (2016) 46–56.

[38] C. Cai, Z. Zhang, J. Liu, N. Shan, H. Zhang, D.D. Dionysiou, Visible light-assisted heterogeneous Fenton with ZnFe₂O₄ for the degradation of Orange II in water, *Appl. Catal. B-Environ.* 182 (2016) 456–468.

[39] Y. Sheng, Y. Sun, J. Xu, J. Zhang, Y.-F. Han, Fenton-like degradation of rhodamine B over highly durable Cu-embedded alumina: kinetics and mechanism, *AIChE J.* 64 (2) (2018) 538–549.

[40] E.G. Garrido-Ramírez, B.K.G. Theng, M.L. Mora, Clays and oxide minerals as catalysts and nanocatalysts in Fenton-like reactions - a review, *Appl. Clay Sci.* 47 (2010) 182–192.

[41] X. Li, K. Zhu, J. Pang, M. Tian, J. Liu, A.I. Rykov, M. Zheng, X. Wang, X. Zhu, Y. Huang, B. Liu, J. Wang, W. Yang, T. Zhang, Unique role of Mössbauer spectroscopy in assessing structural features of heterogeneous catalysts, *Appl. Catal. B-Environ.* 224 (2018) 518–532.

[42] C.L. Chien, S.H. Liou, D. Kofalt, W. Yu, T. Egami, T.J. Watson, T.R. McGuire, Magnetic properties of Fe_xCu_{100-x} solid solutions, *Phys. Rev. B* 33 (1986) 3247–3250.

[43] X. Chen, J. Wang, K. Yang, C. Meng, C.T. Williams, C. Liang, Structure investigation and dibenzothiophene hydrodesulfurization properties of Fe-substituted Ni-Si intermetallics, *J. Phys. Chem. C* 119 (2015) 29052–29061.

[44] Y. Lei, C.-S. Chen, Y.-J. Tu, Y.-H. Huang, H. Zhang, Heterogeneous degradation of organic pollutants by persulfate activated by CuO-Fe₃O₄: mechanism, stability, and effects of pH and bicarbonate ions, *Environ. Sci. Technol.* 49 (2015) 6838–6845.

[45] H.-J. Wan, B.-S. Wu, C.-H. Zhang, H.-W. Xiang, Y.-W. Li, B.-F. Xu, F. Yi, Study on Fe-Al₂O₃ interaction over precipitated iron catalyst for Fischer-Tropsch synthesis, *Catal. Commun.* 8 (2007) 1538–1545.

[46] E. de Smit, F.M.F. de Groot, R. Blume, M. Havecker, A. Knop-Gericke, B.M. Weckhuysen, The role of Cu on the reduction behavior and surface properties of Fe-based Fischer-Tropsch catalysts, *Phys. Chem. Chem. Phys.* 12 (2010) 667–680.

[47] L. Qi, Q. Yu, Y. Dai, H. Zhang, L. Dong, C. Tang, L. Liu, F. Gao, Y. Chen, Influence of cerium precursors on the structure and reducibility of mesoporous CuO-CeO₂ catalysts for CO oxidation, *Appl. Catal. B-Environ.* 119–120 (2012) 308–320.

[48] B.-C. Jiang, Z.-Y. Lu, F.-Q. Liu, A.-M. Li, J.-J. Dai, L. Xu, L.-M. Chu, Inhibiting 3-dinitrobenzene formation in Fenton oxidation of nitrobenzene through a controllable reductive pretreatment with zero-valent iron, *Chem. Eng. J.* 174 (2011) 258–265.

[49] L. Carlos, D. Fabbri, A.L. Capparelli, A.B. Prevot, E. Pramauro, F.S.G. Einschlag, Intermediate distributions and primary yields of phenolic products in nitrobenzene degradation by Fenton's reagent, *Chemosphere* 72 (2008) 952–958.

[50] D.A. Nichela, A.M. Berkovic, M.R. Costante, M.P. Juliarena, F.S. García Einschlag, Nitrobenzene degradation in Fenton-like systems using Cu(II) as catalyst. Comparison between Cu(II)- and Fe(III)-based systems, *Chem. Eng. J.* 228 (2013) 1148–1157.

[51] J. Bai, Y. Liu, X. Yin, H. Duan, J. Ma, Efficient removal of nitrobenzene by Fenton-like process with Co-Fe layered double hydroxide, *Appl. Surf. Sci.* 416 (2017) 45–50.

[52] S. Zhang, D. Wang, X. Zhang, P. Fan, Zero-valent iron immobilized on multi-walled carbon nanotubes for heterogeneous catalytic ozonation of methylene blue as model compound, *CLEAN-Soil Air Water* 42 (2014) 609–616.

[53] L. Carlos, D. Nichela, J.M. Triszcz, J.I. Felice, F.S. García Einschlag, Nitration of nitrobenzene in Fenton's processes, *Chemosphere* 80 (2010) 340–345.

[54] L. Zhao, J. Ma, Z.-z. Sun, Oxidation products and pathway of ceramic honeycomb-catalyzed ozonation for the degradation of nitrobenzene in aqueous solution, *Appl. Catal. B-Environ.* 79 (2008) 244–253.

[55] H.-M. Hung, F.H. Ling, M.R. Hoffmann, Kinetics and Mechanism of the enhanced reductive degradation of nitrobenzene by elemental iron in the presence of ultrasound, *Environ. Sci. Technol.* 34 (2000) 1758–1763.